*Particle Accelerators*, 1994, Vol. 45, pp. 167–183
Reprints available directly from the publisher
Photocopying permitted by license only

©1994 Gordon and Breach Science Publishers, S.A.
Printed in Malaysia

# TRANSVERSE IMPEDANCE OF A 2-GAP ACCELERATING STRUCTURE IN AN INDUCTION ACCELERATOR

THOMAS C. GENONI and THOMAS P. HUGHES

*Mission Research Corporation, 1720 Randolph, SE, Albuquerque, NM 87106*

*(Received 6 December 1993; in final form 15 March 1994)*

Beam break-up instability (BBU) growth in multigap accelerators is caused by the transverse impedance, $Z_\perp(\omega)$, arising from the interaction between the beam and a dipole mode in the accelerating cavities. In recirculating induction accelerators, such as the Spiral Line Induction Accelerator (SLIA) and the Recirculating Linear Accelerator (RLA), multiple beam pipes pass off-axis through a single radial line feed, resulting in coupling between the accelerating gaps and destroying the cylindrical symmetry usually assumed in calculations of $Z_\perp(\omega)$. Using an eigenmode expansion formalism, we calculate the transverse impedance for two coupled shielded gaps. Our calculations show that the imaginary part of $Z_\perp(\omega)$ can be smaller or larger than the single gap value, depending on the spacing between the gaps. An interpretation of the results is presented in terms of two resonant circuits coupled by a transmission line, and comparison is made to previous coupled oscillator models.

KEY WORDS: Electromagnetic field calculations, impedances, induction accelerators

## 1 INTRODUCTION

The beam break-up instability (BBU) in multigap accelerators involves a resonant interaction between the transverse motion of the beam centroid and a dipole electromagnetic mode in the accelerating cavities.[1] The coupling between the beam and a cavity is specified by the transverse impedance $Z_\perp(\omega)$, which is a complex function of frequency $\omega$. $Z_\perp$ is essentially the Fourier time-transform of the wake-field excited in the cavity by an off-axis charge moving along the beam pipe. For axisymmetric gap geometries such as those in the Advanced Test Accelerator (ATA)[1] and the Sandia ET-2 accelerating module,[2] $Z_\perp$ has been calculated both analytically[3,4,5] and numerically.[6,7]

In recirculating induction accelerators, such as the Spiral Line Induction Accelerator (SLIA)[8] and the Recirculating Linear Accelerator,[9] the calculation of $Z_\perp$ and the analysis of BBU growth is complicated by the presence of multiple accelerating gaps in a single radial line feed. A typical geometry with two shielded gaps is illustrated in Figure 1. To our knowledge, shielded gaps were first used in the Sandia MABE accelerator.[10] Their purpose is to produce axisymmetric accelerating fields in each accelerator gap. The off-axis beam pipe positions destroy the cylindrical symmetry assumed in the $Z_\perp$ calculations cited above.

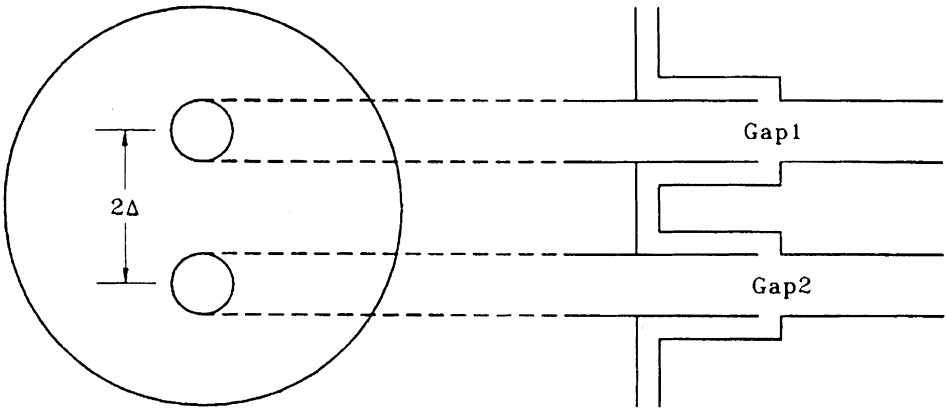


FIGURE 1: Schematic of coupled shielded gap geometry.

Furthermore, the gaps are coupled—passage of the beam through one gap produces fields in the other.

In this paper, we present a calculation of the transverse impedance for two coupled shielded gaps using an eigenmode expansion formalism which effectively treats the radial line and the two gaps as a single cavity responding to the excitation of an off-axis beam passing through one of the gaps. Mode coupling, if present, is thus "built into" the formalism in a self-consistent way. The eigenmode method restricts the treatment to geometries which are composed of rectangular regions (see Figure 1). However, we believe that the model captures the essential effects.

Colombant, Lau, and Chernin (CLC)[11] recently analyzed gap coupling effects using a coupled oscillator model. They concluded that the coupling reduced BBU growth. The calculation presented here indicates that BBU growth may be larger or smaller for coupled cavities depending on the transverse separation of the cavities. We believe that the discrepancy lies in the fact that the CLC model assumes that the transverse impedance and Q-factor of each cavity have the same values in the coupled configuration as they do for single cavities. This means that the second cavity is treated as an additional, complex load on the first cavity. To reproduce the behavior obtained from the field model, we find that one must treat the second cavity as a replacement for part of the original load.

We note that beam recirculation complicates the calculation of BBU growth.[12] A particular cavity may contain fields before the beam enters it because of cross-coupling from an adjacent, previously excited, cavity. We do not consider these effects here.

This paper is organized as follows. In Section 2, the eigenmode expansion formalism is discussed in detail. Section 3 contains numerical results from application of the model to a specific coupled shielded gap geometry similar to that in the SLIA.[8] In Section 4, our results are interpreted in terms of a simple coupled resonant circuit model of $Z_\perp$, similar to the CLC coupled oscillator model. A brief discussion and summary is presented in Section 5.

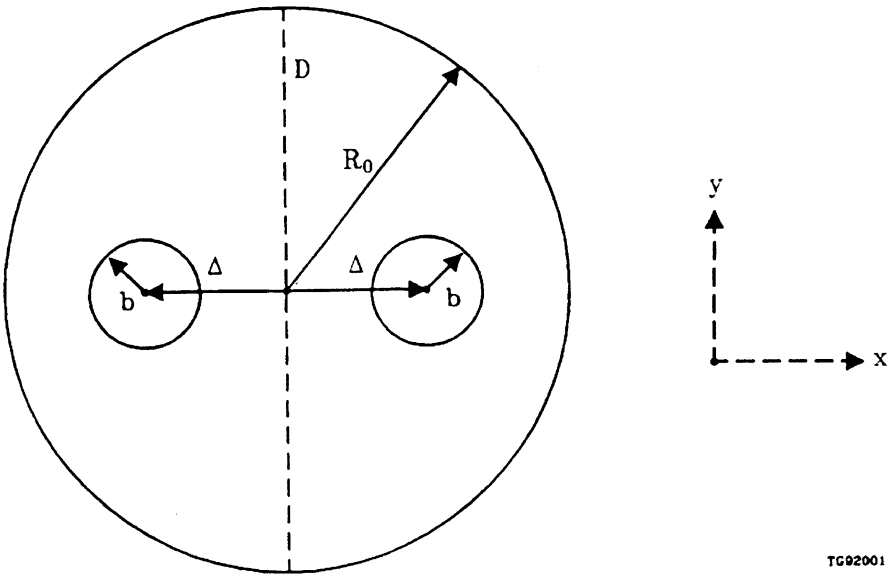


FIGURE 2: Geometry for two-gap calculation.

## 2 FIELD MODEL OF TRANSVERSE IMPEDANCE

A charge moving off-axis through an accelerating gap produces dipole wake fields which exert a time-dependent transverse force on subsequent particles. This time-dependent force from a single charge constitutes a Green's function which is used in the calculation of BBU growth. By transforming to the frequency domain and using eigenmode expansions, the calculation of the transform of the force (the transverse impedance) is reduced to an algebraic problem. In the present work, this technique[3,5,13] is applied to the coupled shielded gap geometry in Figures 1 and 2.

We consider a case with two drift tubes symmetrically offset with respect to a diameter ($D$) of the radial line (Figure 2). We define a cylindrical $(r, \theta)$ coordinate system with its origin at the center of the beam pipe on the right in Figure 2 and $\theta = 0$ along the $x$ axis. The lack of cylindrical symmetry about $r = 0$ means that the fields excited by a displacement in the $x$ direction cannot be obtained just by rotating the fields excited by an equal displacement in the $y$ direction. We must calculate a $Z_{\perp x}(\omega)$ (transverse impedance for $x$ displacements) and a $Z_{\perp y}$. Arbitrary small displacements can be decomposed into $x$ and $y$ displacements and the gap response calculated separately. We anticipate that gap coupling effects will be much stronger for $x$ displacements than for $y$ displacements. For $x$ displacements, the (predominantly) $\cos\theta$ dependence of the excited fields will have a maximum at the position of the second pipe ($\theta = \pi$), while for $Z_{\perp y}$, the (predominantly) $\sin\theta$ dependence of the fields produces a node at $\theta = \pi$, minimizing the effect of the second gap.

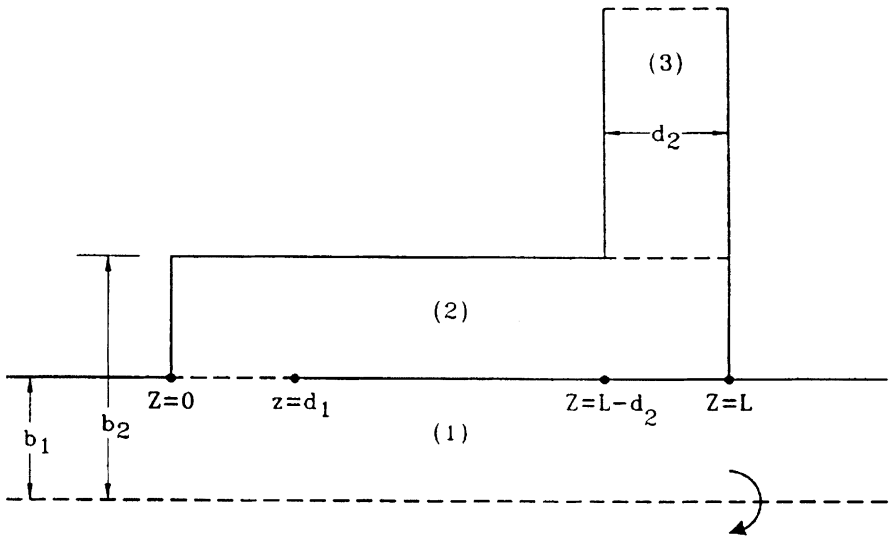


FIGURE 3: Shielded gap geometry divided into regions of rectangular cross-section viz. (1) drift tube, (2) coax, and (3) radial line regions.

Figure 3 shows how the shielded gap is divided into three rectangular regions to obtain expansions for the fields. We now examine each region in turn.

### 2.1 *Drift Tube ($r < b_1$)*

In the drift tube, we represent the TM and TE contributions to the electric and magnetic fields by sums of Fourier integrals:

$$A_z(r, z, \theta) = \sum_{n=0}^{\infty} A_n \cos n\theta \int_{-\infty}^{\infty} \frac{\sin(kd_1/2)}{\pi k} e^{ik(z-d_1/2)} \frac{J_n(qr)}{J_n(qb_1)} dk \tag{1}$$

where $q^2 = \omega^2/c^2 - k^2$

$$B_z(r, z, \theta) = \sum_{n=1}^{\infty} A_n \sin n\theta \int_{-\infty}^{\infty} \frac{\sin(kd_1/2)}{\pi k} e^{ik(z-d_1/2)} \left[\frac{-ikn}{qb_1} \frac{J_n(qr)}{J_n'(qb_1)}\right] dk \tag{2}$$

where $A_z$ is the $z$ component of the vector potential ($E_z = \frac{i\omega}{c} A_z$), and $B_z$ is the $z$ component of the magnetic induction. All of the transverse field components may be obtained from Equations (1) and (2) in the usual fashion.[14]

To obtain Equations (1) and (2), we have followed Briggs et al.[3] in assuming that $A_z$ is constant across the accelerating gaps:

$$A_z(b_1, z, \theta) = \begin{cases} 0 & z < 0,\ z > d_1 \\ \sum_n A_n \cos n\theta & 0 < z < d_1 \end{cases} \tag{3}$$

and that

$$A_\theta(b_1, z, \theta) = 0 \quad -\infty < z < \infty \tag{4}$$

Equations (3) and (4) provide an adequate approximation to the exact matching conditions in the narrow gap case ($d_1 < b_1$). (See Reference 3 for a detailed discussion.) The accuracy of the approximation in the present case is demonstrated by the benchmark calculation present in Section 3 below. Use of Equations (3) and (4) greatly simplifies the mode expansions and field matching conditions at $r = b_1$, at the expense of some generality.

### 2.2 *Coax Region ($b_1 < r < b_2$)*

The Fourier-Bessel expansions for the fields in this region are as follows:

$$A_z(r, z, \theta) = \sum_{n=0}^{\infty} \cos n\theta \sum_{m=0}^{\infty} [D_{nm} J_n(q_m r) + E_{nm} Y_n(q_m r)] \cos k_m z \tag{5}$$

$$B_z(r, z, \theta) = \sum_{n=1}^{\infty} \sin n\theta \sum_{m=1}^{\infty} [F_{nm} J_n(q_m r) + G_{nm} Y_n(q_m r)] \sin k_m z \tag{6}$$

where $k_m = m\pi/L$ and $q_m^2 = \omega^2/c^2 - k_m^2$. Consistent with the discussion following Equation (4), we require that $A_\theta(b_1, z, \theta) = 0$ and $A_\theta(b_2, z, \theta) = 0$, the latter condition limiting the applicability of the model to narrow radial lines ($d_2 < b_2$). Standard Fourier analysis then gives two sets of equations relating the coefficients $D_{nm}$, $E_{nm}$, $F_{nm}$, and $G_{nm}$.

### 2.3 *Radial Line ($b_2 < r$)*

Using the assumption of a narrow radial line we restrict the fields to be TM, represented by a longitudinally uniform $A_z$ (Reference 3):

$$A_z(r, z, \theta) = \sum_{n=0}^{\infty} \cos n\theta \left[ B_n J_n\left(\frac{\omega r}{c}\right) + C_n Y_n\left(\frac{\omega r}{c}\right)\right] \tag{7}$$

We now proceed to apply (a) matching conditions on the tangential fields at $r = b_1$ and $r = b_2$, (b) a lumped impedance boundary condition at the outer boundary of the radial line, and (c) symmetry conditions along the diameter. The matching condition at $r = b_1$ again follows Briggs et al.[3] The return current in the drift tube wall due to the off-axis beam is interrupted by the accelerating gap. We impose a discontinuity in $B_\theta$ equal to the dipole wall current:

$$B_\theta^{(2)}(b_1, z, \theta) - B_\theta^{(1)}(b_1, z, \theta) = \frac{4I\xi}{cb_1^2} e^{i\omega/c} \cos\theta \quad (0 < z < d_1) \tag{8}$$

where $I$ is the beam current and $\xi$ is the displacement of the beam centroid from the axis of the drift tube.

Continuity of $A_z$ at $r = b_1$ requires

$$\sum_{m=0}^{\infty} [D_{nm} J_n(q_m b_1) + E_{nm} Y_n(q_m b_1)] \cos k_m z = \begin{cases} 0 & d_1 < z < L \\ A_n & 0 < z < d_1 \end{cases} \tag{9}$$

At $r = b_2$, $A_z$ and $B_\theta$ are continuous across the opening to the radial line, giving

$$\sum_{m=0}^{\infty} [D_{nm} J_n(q_m b_2) + E_{nm} Y_n(q_m b_2)] \cos k_m z = \begin{cases} 0 & 0 < z < L - d_2 \\ B_n J_n\left(\frac{\omega b_2}{c}\right) + C_n Y_n\left(\frac{\omega b_2}{c}\right) & L - d_2 < z < L \end{cases} \tag{10}$$

$$B_\theta^{(2)}(b_2, z, \theta) = B_\theta^{(3)}(b_2, z, \theta) \qquad L - d_2 < z < L \tag{11}$$

At the outer boundary to the radial line (radius $R_0$ in Figure 2), a lumped impedance boundary condition is applied:

$$E_z = -Z_s B_t \qquad L - d_2 < z < L \tag{12}$$

where $B_t$, the magnetic field tangential to the outer boundary, is in general a linear combination of $B_r$ and $B_\theta$. If we define a second cylindrical coordinate system $(r', \theta')$ with its origin at the center of the radial line (Figure 4), we see that $B_t$ can be written as

$$B_t = B_\theta \cos(\theta - \theta') + B_r \sin(\theta - \theta') \tag{13}$$

where $B_\theta$, $B_r$ are evaluated along the boundary. Since this boundary is not a coordinate curve ($r$ = constant) of the $(r, \theta)$ coordinate system, Equation (12) couples all modes together.

Finally, we apply symmetry conditions along the diameter D in Figure 2. Assuming an excitation due to an off-axis beam in one of the gaps, we note that the symmetry makes it possible to carry out the calculation using expansions for the fields on only one side of the diameter D. The complete solution for the fields (on the side of D

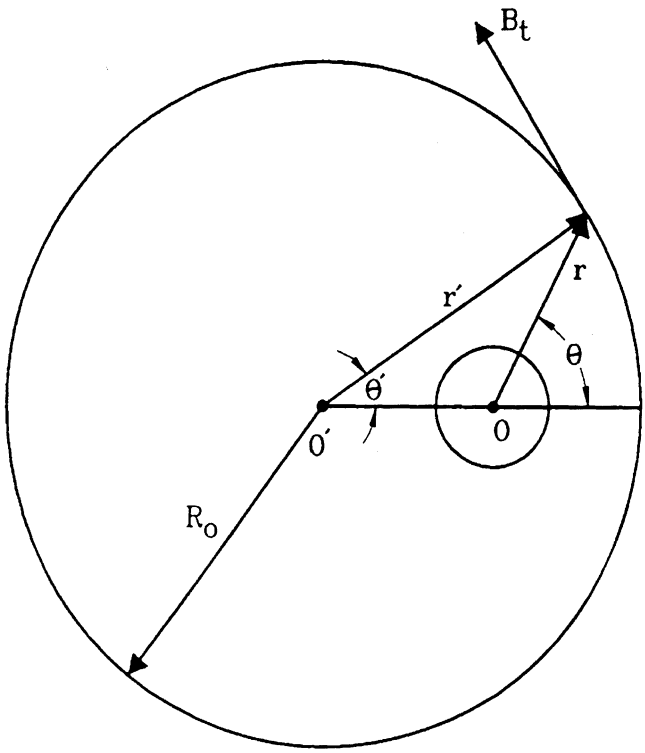


FIGURE 4: Schematic of off-axis pipe showing $B_t$ tangent to outer boundary at $r'=R_0$.

through which the beam is assumed to pass) is the average of the two solutions corresponding to symmetric and antisymmetric boundary conditions applied along D. (The symmetric condition is $\partial A_z/\partial x = 0$, and the antisymmetric is $A_z = 0$.) For this case, the complete outer boundary consists of the semicircle at $r' = R_0$, $-\pi/2 \leq \theta' \leq \pi/2$, and the diameter D. In practice, the infinite sum in Equation (7) is truncated at some maximum value $n = N$. The symmetry condition is applied at $M$ equally spaced points along D, and Equation (12) is applied at $N + 1 - M$ points along the semicircle at equal $\theta'$ spacings. A ratio of $(N + 1 - M)/M = 3/2$ proved satisfactory.

Standard Fourier analysis on the matching and boundary conditions discussed above leads to a system of linear equations which are solved numerically for the expansion coefficients in Equations (1) and (5) through (7). Examination of the fields within the drift tube region shows that only the $n = 1$ terms in the expansions in Equations (1) and (2) contribute to the on-axis transverse force experienced by a beam particle traversing the gap. Integration of the force along the path $r = 0$, $-\infty < z < \infty$ yields the following expression for the transverse impedance as a function of angular frequency $\omega$:

$$Z_\perp(\omega) = \frac{1}{b_1}\int_0^{d_1} A_1 e^{-i\omega z/c} dz \Big/ \left(\frac{I\xi}{cb_1}\right)$$

$$= A_1 \frac{d_1}{b_1} \frac{\sin(\omega d_1/2c)}{\omega d_1/2c}\, e^{-i\omega d_1/2c} \Big/ \left(\frac{I\xi}{cb_1}\right) \tag{14}$$

Multiplication by $30/b_1$ (cm) gives the transverse impedance in units of Ω/cm.

## 3 NUMERICAL RESULTS FROM FIELD MODEL

We now present results obtained from the model in Section 2 for the cavity parameters in Table 1. These parameters are based on those of the SLIA accelerator.

TABLE 1: Shielded gap parameters.

| | (cm) |
|---|---|
| Beam pipe radius, $b_1$ | 5.72 |
| Coax radius, $b_2$ | 7.2 |
| Coax length, $L$ | 20. |
| Gap width, $d_1$ | 2.0 |
| Radial line width, $d_2$ | 2.0 |

The value of 2 cm for the accelerating gap is significantly smaller than in the SLIA, which uses a long tapered gap. This difference mainly affects the behavior of the so-called trapped mode.[4] By its nature, this mode is expected to exhibit negligible cross-coupling. As a further simplification, we have used an outgoing-wave boundary condition to terminate the radial line (i.e., $Z_s = Z_0$ where $Z_0$ is the impedance of free space). Our results are obtained by carrying out a numerical solution of the system of equations in Section 2. Since asymptotic BBU growth is determined by the peak value of the imaginary part of $Z_\perp(\omega)$, we will show only plots of $\mathrm{Im}[Z_\perp(\omega)]$.

We first benchmarked the model by applying it to the calculation of the transverse impedance of a single, on-axis shielded gap with the parameters in Table 1. Recall that the model uses a single term in the expansion for $A_z$ in the gap and radial line regions—$A_z$ is assumed to be uniform in these regions. Figure 5 shows $\mathrm{Im}[Z_\perp(\omega)]$ calculated from the present model compared to a calculation using the code BBUS,[15] which does not assume uniform $A_z$ in the gaps and radial line. We see that there is no significant difference between the two calculations. The function $\mathrm{Im}[Z_\perp(\omega)]$ has a

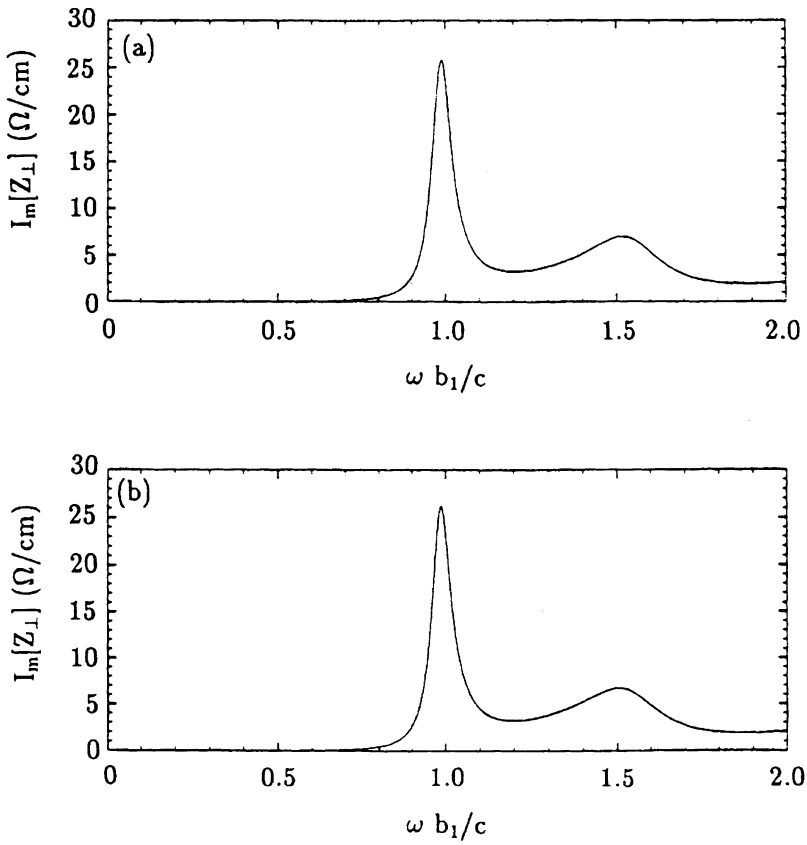


FIGURE 5: Imaginary part of transverse impedance for single on-axis shielded gap (parameters of Table 1) calculated using (a) exact $A_z$ and (b) approximate (constant) $A_z$ in the drift-tube gap and in the radial line.

large peak near $\omega b_1/c = 0.99$ which we call the fundamental coax mode. It is the lowest order TE standing wave in the coax region, lying just above the TE cutoff of the coax line, and has been seen in previous calculations[15] and experiments.[16] (There are no modes below the coax TE cutoff.) We focus on this mode in the two-gap calculations which follow since it is the dominant contributor to BBU growth.

A series of calculations was carried out for varying values of pipe separation $2\Delta$ (see Figure 2) using the cavity dimensions in Table 1. Results for $\mathrm{Im}[Z_{\perp x}(\omega)]$ in the vicinity of the fundamental coax mode frequency are shown in Figures 6 and 7. These show that the presence of the second gap strongly modifies $Z_{\perp x}(\omega)$. For $\Delta = 15.92$ cm (Figure 7), the peak value of $\mathrm{Im}[Z_{\perp x}(\omega)]$, denoted by $Z_{\perp x}^{\max}$, is about 25 percent smaller than the value for a single gap. Reduction in $Z_{\perp x}^{\max}$ occurs only over a narrow range of $\Delta$ values, however. In Figure 8, we show values of $Z_{\perp x}^{\max}$ and $Z_{\perp y}^{\max}$ as a function of $\Delta$.

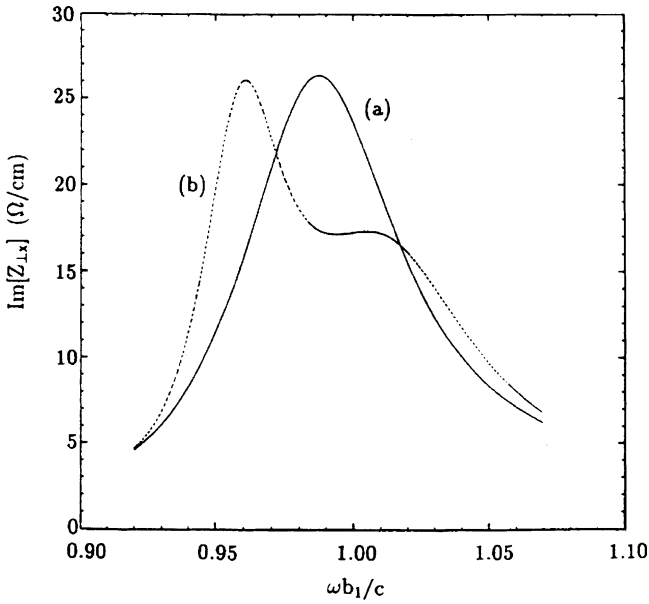


FIGURE 6: Imaginary part of transverse impedance $Z_{\perp x}(\omega)$ for (a) single shielded gap and (b) two coupled gaps with $\Delta$=15 cm.

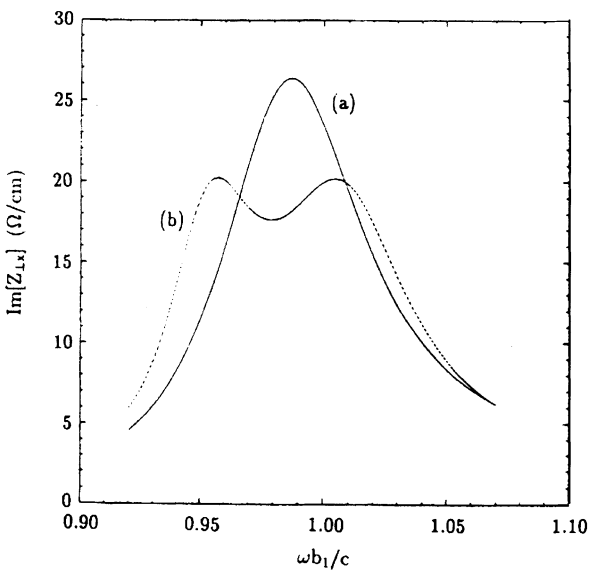


FIGURE 7: Imaginary part of transverse impedance $Z_{\perp x}(\omega)$ for (a) single shielded gap and (b) two coupled gaps with $\Delta$=15.92 cm.

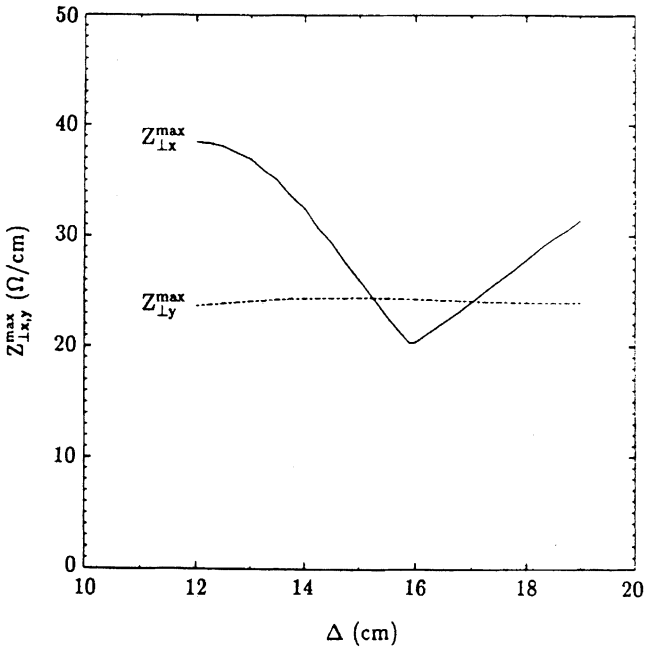


FIGURE 8: $Z_{\perp x}^{max}$ and $Z_{\perp y}^{max}$ (maximum imaginary impedances) as functions of pipe separation for parameters in Table 1. (Outer boundary was at $R_0$=34.5cm.)

On either side of $\Delta = 15.92$ cm, $Z_{\perp x}^{max}$ rises fairly sharply to values larger than the single gap values. We defer further discussion of $Z_{\perp x}^{max}$ in Figure 8 until Section 4, except to note that at $\Delta = 15.92$ cm, the pipe separation corresponds to roughly half of a free-space wavelength of the mode. As anticipated, $Z_{\perp y}^{max}$ is relatively insensitive to the presence of the second gap.

## 4 COUPLED RESONANT CIRCUIT MODEL OF $Z_\perp$

We now present an interpretation of the preceding results using equivalent circuits. In principle, we could derive a circuit model for the configuration in Figure 2 taking the radial line geometry into account (see, e.g., Chapter 8 of Reference 17). For the sake of simplicity, we base the circuit model on the geometry in Figure 9, where the radial line has been replaced by uniform rectangular waveguides. The placement of the waveguides is intended to suggest the $\cos\theta$ dependence of the fields excited by horizontal beam displacements. The key to understanding the results in Figure 8 is that in Figure 9 (and Figure 2), the second cavity is not an additional load which has been added to the first cavity—it *replaces* part of the load on the first cavity.

We can represent a single cavity using the shunt resonant circuit in Figure 10. We prescribe the following correspondences between the mode parameters (resonant

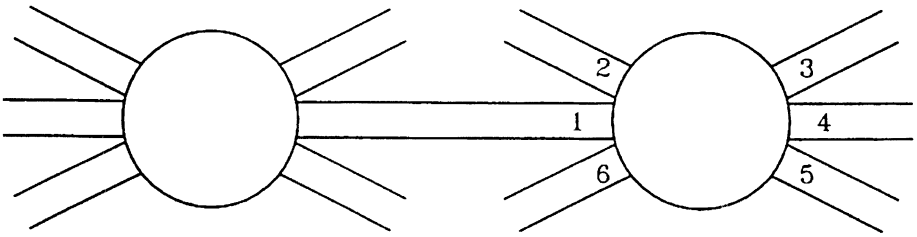


FIGURE 9: Schematic of coupled gap geometry used as basis for equivalent circuit model. The radial line has been replaced by rectangular waveguides.

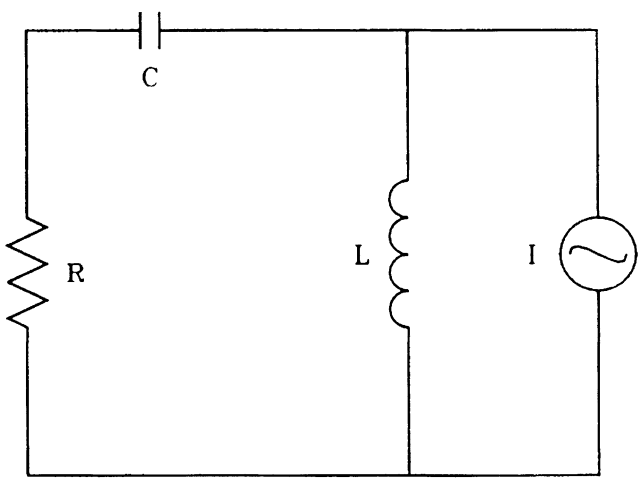


FIGURE 10: Resonant circuit model for single mode.

frequency $\omega_0$, peak value of $\mathrm{Im}[Z_\perp(\omega)]$, denoted by $Z_\perp^{\max}$, and mode quality factor $Q$) and the circuit parameters $R$, $L$, $C$, and $V_c$ (voltage across the capacitor):

$$\omega_0^2 = 1/LC \tag{15}$$

$$Q = \sqrt{L/C}/R \tag{16}$$

$$Z_\perp^{\max} = L/RC \tag{17}$$

$$Z_\perp(\omega) \equiv \frac{\omega_0 V_c}{i\omega I} = \frac{Z_\perp^{\max}\,\omega_0^2/Q}{\omega_0^2 - \omega^2 - i\omega\omega_0/Q} \tag{18}$$

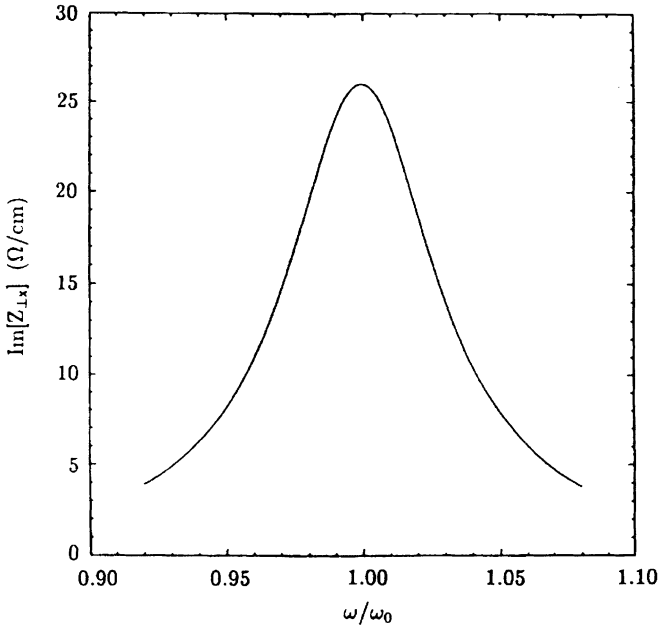


FIGURE 11: Imaginary part of the transverse impedance from resonant circuit of Figure 10 for single mode ($Z_\perp^{\max}$=26, $Q$=15).

A plot of $Z_\perp(\omega)$ from Equation (18) for $f_0 = 830$ MHz, $Z_\perp^{\max} = 26$, and $Q = 15$ is shown in Figure 11. With these parameters, the resonant circuit closely follows curve (a) of Fig. 6, i.e., the impedance of a single cavity.

To model the coupled cavities in Figure 9, we consider two identical resonant circuits connected by a transmission line of length $\ell$ (see Figure 12). We take $\ell$ to correspond to the distance between the coaxial regions of the two accelerating gaps [$\ell = 2(\Delta - b_2)$]. The transmission line and coupled circuit of Figure 12(a) can be replaced by an equivalent impedance

$$Z_{eq} = Z_0 \frac{Z_L - iZ_0 \tan(\omega\ell/c)}{Z_0 - iZ_L \tan(\omega\ell/c)} \tag{19}$$

where $Z_0$ is the characteristic impedance of the transmission line and

$$Z_L = -i\omega L + R' - \frac{1}{i\omega C} \tag{20}$$

producing the equivalent circuit of Figure 12(b). We relate the transverse impedance to the voltage across the capacitor as before.

It remains to specify the characteristic impedance $Z_0$ and the circuit resistance $R'$. The impedance of a microwave element is directly proportional to the Poynting flux

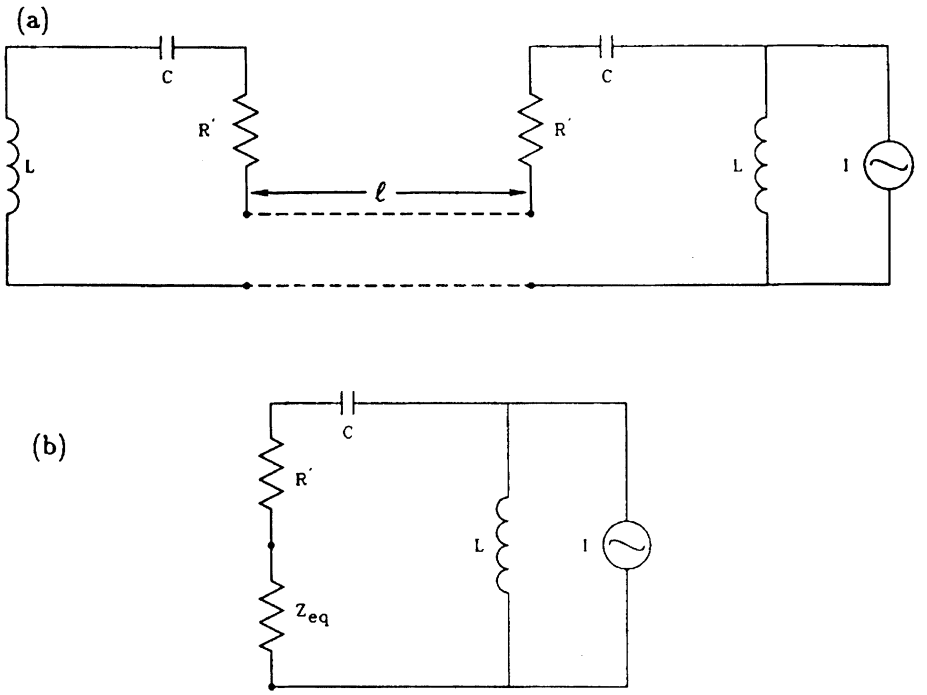


FIGURE 12: The coupled resonant circuits connected by a transmission line in (a) are equivalent to the circuit in (b) where $Z_{eq}$ is given by Equations (19) and (20).

into it (Chapter 5 in Reference 17). In Figure 9, the characteristic impedance of the $i^{th}$ waveguide is given by $\alpha_i R$ where $\alpha_i$ is the fraction of the total Poynting flux that it carries, and $R$ is the total impedance for a single cavity. Thus, we have $Z_0 = \alpha_1 R$ and $R' = (1 - \alpha_1)R$. Noting the $\cos\theta$ dependence of the (primarily) $n = 1$ mode in question, we estimate the parameter $\alpha_1$ as follows:

$$\alpha_1 = \frac{1}{\pi} \int_{-\theta_1}^{\theta_1} \cos^2\theta \, d\theta \simeq \frac{2\theta_1}{\pi} \tag{21}$$

where $2\theta_1 \simeq b_1/\Delta$ is the angle subtended by the second cavity, and the small angle approximation has been used.

Results from this model for $Z_\perp^{\max}$ as a function of $\Delta$ (or equivalently $\ell$) are shown in Figure 13 and are compared to results from the field calculation. The outer boundary radius $R_0$ was set to 100 cm. Since the lumped impedance outer boundary condition is nearly perfectly transmitting ($Z_s = Z_0$), the precise value of $R_0$ has a minimal effect on the results. The coupled circuit model produces results qualitatively similar

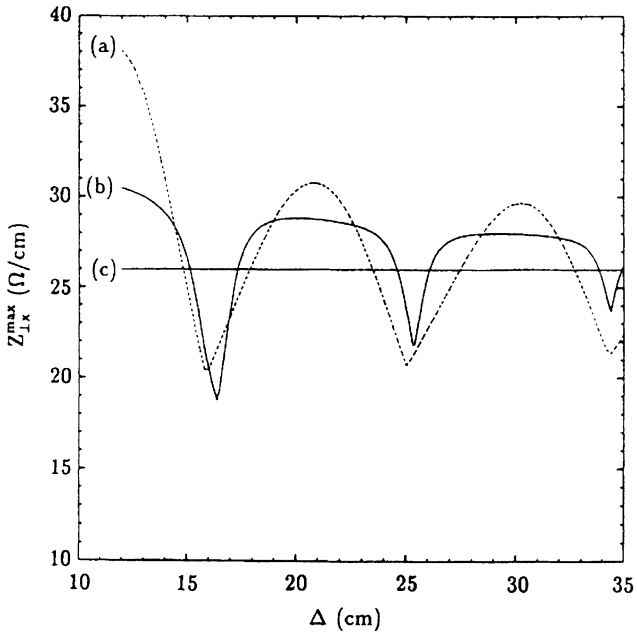


FIGURE 13: $Z_{\perp x}^{\max}$ versus $\Delta$ from (a) mode expansion calculations (parameters in Table 1) and (b) coupled circuit model. Horizontal line (c) shows value for single on-axis gap.

to the eigenmode expansion calculations. The cross-coupling effect decreases with increasing $\Delta$, and values of $Z_{\perp x}^{\max}$ smaller or larger than the single gap value can result depending on the gap spacing. The latter implies that asymptotic BBU growth for coupled gaps will be greater or less than for uncoupled gaps depending on $\Delta$. This result differs from the conclusion of the CLC model,[11] and we discuss the reasons for this in the following section. The minima in $Z_{\perp x}^{\max}$ occur for

$$\Delta \approx b_2 + \frac{1}{4} n \lambda_f \,, \qquad n = 1, 2, \cdots \tag{22}$$

where $\lambda_f = 2\pi c/\omega_0$ is the free-space wavelength of the resonant mode.

## 5 DISCUSSION

The main results of the field model can be summarized as follows. Two transverse impedances, $Z_{\perp x}$ and $Z_{\perp y}$ are needed to describe the dipole response of the two coupled gaps. Only one of these, $Z_{\perp x}$, is strongly affected by the second gap. The qualitative behavior of $Z_{\perp x}$ can be reproduced using a circuit model.

Our circuit model and the CLC model[11] are mathematically equivalent. However, the CLC model assumes $R' = R$ and treats the cross-coupling strength (proportional to $\alpha_1 R$ in our model) as a free parameter. The assumption $R' = R$ means that the second cavity acts as an additional energy-loss mechanism for the first cavity. It is not too surprising that this leads to reduction of BBU growth for the coupled system. By setting $R' = R$, we can indeed reproduce the CLC results with the circuit model of Section 4. In Figure 13, we find that curve (b) moves down so that it always lies below curve (c), i.e., $Z_{\perp x}^{\max}$ is always lower for coupled gaps than for single gaps.

The field model indicates that $R' = R$ is not a valid assumption for the coupled gap geometry in Figure 1. Our findings, however, do not rule out this possibility in general. For example, Menge et al.[18] report reduced BBU growth in an experiment using loop-coupled cavities. We believe that in this case one can plausibly assume $R' = R$, since the coupling loops do not affect the loss mechanism which gives rise to the finite $Q$ of the uncoupled cavities. (The cavities contained microwave-absorbing material.)

The main practical implication of our results is that the transverse spacing of shielded gaps can have a large effect on their transverse impedance.

## ACKNOWLEDGEMENTS

We thank John Edighoffer and Sid Putnam for useful discussions.

This work was supported by the Defense Advanced Research Projects Agency, under ARPA Order No. 7792, and monitored by the Naval Surface Warfare Center.

## REFERENCES

1. V.K. Neil, L.S. Hall, and R.K. Cooper, *Particle Accelerators*, **9** (1979) 213.
2. W.K. Tucker, S.L. Shope, and D.E. Hasti, in *Proceedings of the 1987 IEEE Particle Accelerator Conference*, Cat. No. 87CH2387-9 (IEEE, New York, 1987) p.957.
3. R.J. Briggs, D.L. Birx, G.J. Caporaso, V.K. Neil, and T.C. Genoni, *Particle Accelerators*, **18** (1985) 41.
4. J.F. DeFord, in *Proceedings of the 1990 Linear Accelerator Conference*, LA-12004-C (Los Alamos National Laboratory) p.375.
5. T.C. Genoni and T.P. Hughes, *Phys. Rev. A15*, **46** (1992) 5174 (Appendix).
6. R.B. Miller, B.M. Marder, P.D. Coleman, and R.E. Clark, *J. Appl. Phys.*, **63** (1988) 997.
7. G.D. Craig, in *Proceedings of the 1990 Linear Accelerator Conference*, LA-12004-C (Los Alamos National Laboratory) p. 381.
8. V. Bailey, P. Corcoran, J. Edighoffer, J. Fockler, J. Lidestri, S. Putnam, and M. Tiefenback, in *Proceedings of the Society of Photo-Optical Instrumentation Engineers*, SPIE Vol. 1407 (1991).
9. M.G. Mazarakis, D.L. Smith, J.W. Poukey, J.S. Wagner, L.F. Bennett, W.R. Olson, B.N. Turman, K.R. Prestwich, and J. Wells, in *Conference Record of the 1991 IEEE Particle Accelerator Conference* (IEEE, New York, 1991) p.3126.
10. P.D. Coleman, J.J. Ramirez, D.E. Hasti, T.W.L. Sanford, J.W. Poukey, C.W. Huddle, A.W. Sharpe, L.L. Torrison, J.A. Alexander, and C.E. Heath, *IEEE Trans. Nucl. Sci.*, **NS-32** (1985) 3268.
11. D. Colombant, Y.Y. Lau, and D. Chernin, *Particle Accelerators*, **35**, (1991) 193. See also D.G. Colombant and Y.Y. Lau, *J. Appl. Phys.*, **72** (1992) 3874.
12. D. Colombant and Y.Y. Lau, *Nucl. Instr. and Meth.*, **A31**, 1 (1992) and references therein.
13. H. Henke, *IEEE Trans. Nucl. Sci.*, **NS-32**, (1985) 2335.

14. J.D. Jackson, *Classical Electrodynamics* (Wiley, New York, 1962), pp. 241–2.
15. T.C. Genoni, unpublished.
16. J. Edighoffer, private communication.
17. C.G. Montgomery, R.H. Dicke, and E.M. Purcell, eds., *Principles of Microwave Circuits* (Dover, New York, 1965).
18. P.R. Menge, R.M. Gilgenbach, and Y.Y. Lau, *Phys. Rev. Lett.*, **69**, (1992) 2372.